Identifying the seizure onset zone with intracranial EEG: A systematic comparison between power and connectivity-based biomarkers

Manel Vila-Vidal, Ferran Craven-Bartle Corominas, Matthieu Gilson, Riccardo Zucca, Alessandro Principe, Rodrigo Rocamora, Gustavo Deco, Adrià Tauste Campo

Identifying the seizure onset zone with intracranial EEG: A systematic comparison between power and connectivity-based biomarkers

Manel Vila-Vidal*[1,a,b], Ferran Craven-Bartle Corominas[1,a], Matthieu Gilson[c], Riccardo Zucca[b,d,e], Alessandro Principe[d,f,g], Rodrigo Rocamora†[d,f,g], Gustavo Deco[2,b,h], and Adrià Tauste Campo[2,a]

[1]These authors equally contributed to this work
[2]These authors jointly supervised this work
[a]Computational Biology and Complex Systems, Department of Physics, Universitat Politècnica de Catalunya, 08028, Barcelona, Spain
[b]Center for Brain and Cognition, Department of Information and Communication Technologies, Universitat Pompeu Fabra, 08005, Barcelona, Spain
[c]Institut de Neurosciences des Systèmes (INS, UMR1106), INSERM-AMU, 13005 Marseille, France
[d]Hospital del Mar Medical Research Institute, 08003, Barcelona, Spain
[e]Donders Centre for Neuroscience, Radboud University, Nijmegen, Netherlands
[f]Faculty of Health and Life Sciences, Universitat Pompeu Fabra, 08003, Barcelona, Spain
[g]Epilepsy Monitoring Unit, Department of Neurology, Hospital del Mar, 08003, Barcelona, Spain
[h]Institució Catalana de Recerca i Estudis Avançats, 08010, Barcelona, Spain

*Corresponding author. Address: Computational Biology and Complex Systems, Department of Physics, Universitat Politècnica de Catalunya, 08028, Barcelona, Spain. E-mail: m@vila-vidal.com
†Corresponding author. Address: Hospital del Mar Medical Research Institute, 08003, Barcelona, Spain. E-mail: rrocamora@parcdesalutmar.cat

Abstract

Background: Intracranial EEG biomarkers are under investigation to help localize the seizure onset zone (SOZ) using ictal activity. Existing methods: Biomarkers developed to date can be classified depending on whether they target abnormalities in signal power or the functional connectivity between signals, and they may be optimized depending on the frequency and the time window of interest. New method: This work aimed to systematically compare the performance of power- and connectivity-based biomarkers to identify SOZ contacts from ictal iEEG recordings as a function of these parameters. To do so, we use a previously introduced power-based measure, the normalized mean activation (nMA), which quantifies the average power activation with respect to baseline activity in a frequency band and time window of interest. Similarly, we define the normalized mean strength (nMS), to quantify the mean functional connectivity (cross-correlation) of every contact with the rest of the signals in a frequency band and time window of interest. Results: The biomarker comparison was performed on a dataset of 67 seizures from 10 patients with pharmacoresistant temporal lobe epilepsy. Our results suggest that power-based biomarkers generally perform better for the detection of SOZ than connectivity-based ones. However, a similar performance level can be achieved when both biomarkers are independently optimized over frequency bands and time windows. Optimal performance was achieved in broadband or in the beta range for power-based biomarkers, and in the lower-gamma range for connectivity. Both biomarkers maximized their performance when using a 20-30 s period after seizure onset. Conclusions: The results of this study highlight the importance of this optimization step when comparing different SOZ discrimination biomarkers. This information should be considered when designing seizure onset zone algorithms in clinical applications.

Keywords: Epilepsy, Intracranial EEG, SEEG, Seizure onset zone identification, Power spectrum analysis, Functional connectivity

1 Introduction

Presurgical evaluation of drug-resistant epilepsy often involves the use of intracranial EEG (iEEG) to accurately localize the seizure onset zone (SOZ) (Bancaud, 1980). Recordings from hundreds of sensors are continuously acquired for up to three weeks and visually inspected by highly specialized neurologists. This can be a very challenging procedure given that seizure onset patterns may involve several frequencies (Perucca et al., 2014; Lagarde et al., 2016; Vila-Vidal et al., 2020) and may have complex spatial distributions (Bartolomei et al., 2017).

Several iEEG biomarkers have been developed to help localize the SOZ using ictal activity. These biomarkers can be classified into two groups, depending on their target features: power or connectivity (for an extensive review see (Vila-Vidal and Tauste Campo, 2023)). On one hand, power-based biomarkers target abnormal activity patterns that might correlate with the SOZ. These methods are based on a spectral analysis of the iEEG signals of each region, from which changes or activations at specific frequencies are then extracted and evaluated. Some methods in this group, such as the Epileptogenicity Index (Bartolomei et al., 2008), rely on detecting changes at specific frequency bands, often in the beta and gamma ranges (David et al., 2011; Murphy et al., 2017). Other methods offer more flexibility and can adapt to or combine different frequencies of interest (Gnatkovsky et al., 2011, 2014; Vila-Vidal et al., 2017, 2020).

On the other hand, connectivity-based biomarkers target abnormal changes in functional connectivity, i.e., statistical dependencies of signals between pairs of electrodes. The rationale behind this approach is based on a conceptualization of epilepsy as a disease affecting a network of interconnected regions that generate and propagate ictal activity across the brain (Bartolomei et al., 2017). Different types of statistical relationships have been used to build biomarkers that capture alterations in these functional relationships during ictal periods (Gotman and Levtova, 1996; Bartolomei et al., 2004; Mierlo et al., 2013; Nahvi et al., 2023; Balatskaya et al., 2020).

The studies mentioned above built their biomarkers based on either power or connectivity alone. One of the few exceptions in this regard is the work done by (Balatskaya et al., 2020), which combined the two types of measures to define a joint biomarker. A major limitation of this study, however, was the use of a predefined frequency band (beta-gamma range) and a predefined period of interest (20-30 s after seizure onset), which may fall short of capturing relevant activity given the heterogeneity observed across seizures (Perucca et al., 2014; Lagarde et al., 2016). Up to now, no study has systematically explored the performance of these biomarkers as a function of spectral parameters such as the frequency and the time of interest.

This study aimed to systematically compare the performance of power- and connectivity-based biomarkers to identify SOZ contacts from ictal iEEG recordings. As a general power-based measure, we used the normalized mean activation (Vila-Vidal et al., 2017), which quantifies the average power activation with respect to baseline activity in a frequency band and time window of interest. For the sake of comparison, we defined an analogous connectivity-based measure based on the cross-correlation (Mierlo et al., 2014;

Khambhati et al., 2017). The normalized mean strength (nMS) corresponds to the mean functional connectivity (cross-correlation) of every contact with the rest of signals in a frequency band and time window of interest. Optimal frequency bands and time windows to identify the SOZ may be different for both types of measures. To account for such potential differences, we assessed the discrimination power of both metrics across various frequency bands and time windows of interest and selected the combination that maximized the observed effect in each case independently. This method was tested with a dataset of 67 seizures from 10 patients diagnosed with pharmacoresistant temporal lobe epilepsy that underwent stereo-electroencephalography (SEEG), a particular type of intracranial EEG technique (Talairach et al., 1974; Munari and Bancaud, 1985; Guenot et al., 2001; Cardinale et al., 2013).

2 Methodology

2.1 Patients and recordings

In this study, we analyzed SEEG recordings from a total of 67 seizures from 10 patients with pharmacoresistant focal-onset epilepsy who underwent presurgical evaluation at the Epilepsy Centre of Hospital del Mar (Barcelona, Spain) between 2012 and 2017. In this study, we included only patients for which epileptologists had marked a single and spatially confined seizure onset zone. Patients' characteristics are summarised in Table 1. Seizure onset and termination times were marked by two epileptologists using standard clinical assessment and a consensus decision was reached. For each seizure we analyzed SEEG recordings from the marked ictal epoch together with 60 s of pre-ictal and 60 s of post-ictal epochs.

Stereo-EEG monitoring was performed using a standard clinical intracranial EEG system (XLTEK, a subsidiary of Natus Medical) with a sampling rate of 500 Hz,(in patient P3, the sampling rate was 250 Hz). Recordings were obtained using intracranial multichannel electrodes (Dixi Medical, Besançon, France; diameter: 0.8 mm; 5–15 contacts, 2 mm long, 1.5 mm apart) that were stereotactically inserted using robotic guidance (ROSA, Medtech Surgical, Inc). The decision to implant, the selection of the electrode targets and the implantation duration were entirely made on clinical grounds.

2.2 Data preprocessing

EEG signals were processed in the referential recording configuration (i.e., each signal was referred to a common reference). The electrodes per patient included in the analysis are reported in Table 1. We visually identified noisy electrodes and removed them from the analysis. Signals were band-pass filtered between 1 to 150 Hz using a zero-phase FIR filter (53 dB stopband attenuation, maximal ripples in passband 2%) to remove slow drifts and aliasing effects. A notch filter was applied to 50 Hz and its multiples to remove the power line interference (band-stop FIR filter with band-stop width of 1/10 and 1/35 of the central frequency for 50 Hz and its harmonics, respectively; 53 dB attenuation at center frequency, maximal ripples in passband 2 %).

2.3 General procedure

Our approach was to define and systematically compare two biomarkers, one based on signal power and the other based on functional connectivity, to identify the seizure onset zone in the cohort of patients described above. The first biomarker used in this study is the previously introduced normalized mean activation (nMA) (Vila-Vidal et al., 2017, 2020). The nMA quantifies the average power activation of each contact with respect to baseline activity within a frequency band and time window of interest. Similarly, we defined the normalized mean strength (nMS) to quantify each contact's average functional connectivity strength (i.e., its average functional connectivity to all other contacts) over the same time-frequency ranges. The rationale is that, instead of and in parallel to changes in signal power at electrode contacts, the statistical dependencies of signals between pairs of contacts may change differently depending on each contact's location with respect to the SOZ (Bartolomei et al., 2004; Varotto et al., 2012; Mierlo et al., 2013). In addition, these changes are known to evolve over time (Courtens et al., 2016) and using different temporal windows may capture different stages of the seizure and its propagation.

Both biomarkers are thus expected to depend on frequency bands and time windows and thus their respective level of SOZ discrimination might be optimized over the time-frequency space. We defined 6 frequency bands of interest (FOIs) and 9 time windows of interest (TOIs) to account for this parameter-dependence. FOIs were defined based on canonical bands: broadband (3-160 Hz), δ-θ (3-8 Hz), α (8-12 Hz), β (12-30 Hz), low-γ (30-70 Hz) and high-γ (70-160) Hz. All time windows of interest started at the annotated seizure onset time (reference time, 0 s) and were defined by 9 different window lengths: 0-1 s, 0-2 s, 0-3 s, 0-4 s, 0-5 s, 0-10 s, 0-20 s, 0-30 s and whole seizure. Seizure onset zone discrimination was independently evaluated for all possible FOI-TOI combinations with nMA and nMS. The processing steps for each biomarker are described in the following paragraphs.

2.4 Power-based biomarker: normalized mean activation

The processing used to compute the normalized mean activations (nMA) in each FOI and TOI was very similar to previous works (Vila-Vidal et al., 2017, 2020). In brief, signals were first filtered in 42 non-overlapping logarithmically-spaced narrow frequency bands, each with a bandwidth of 10% of its lower frequency bound, covering the whole spectrum of interest 3-160 Hz. The Hilbert transform was then used to obtain the continuous power in each narrow band. Summation of signal power across narrow bands was used to obtain the total power of each contact in each FOI. Note that using a fixed bandwidth of 10% determines the cutting points of each band, which causes the resulting bands to have small deviations from the predefined FOIs. The resulting cutting points were: $3, 7.8, 12.5, 29.5, 69.7, 160$. Following (Vila-Vidal et al., 2017), we used a pre-ictal baseline of activity from 60 to 20 s before ictal onset. Baseline power values from all contacts were pooled together to build a baseline distribution. We then normalized each contact's power with respect to this baseline and defined the instantaneous activation

as the resulting z-score. This procedure was independently done for each FOI.

The mean activation ($\mathrm{MA}_{i,f,t}$) was then defined for each FOI f, TOI t and contact i as the average of its instantaneous activation in FOI f and across TOI t. This step was repeated for each seizure, thus obtaining a mean strength profile across contacts for each seizure, frequency, and time of interest. To allow for cross-seizure comparison, we normalized mean activation values within each seizure, frequency, and time of interest. We computed the mean $\mu_{\mathrm{MA},f,t}$ and standard deviation $\sigma_{\mathrm{MA},f,t}$ of MA values in each frequency f and time window t across contacts. We then defined the normalized mean activation (nMA) for each contact i, FOI f and TOI t as the z-score the mean strength:

$$\mathrm{nMA}_{i,f,t} = \frac{\mathrm{MA}_{i,f,t} - \mu_{\mathrm{MA},f,t}}{\sigma_{\mathrm{MA},f,t}} \tag{1}$$

2.5 Functional connectivity-based biomarker: normalized mean strength

We first filtered each contact's signal in the six FOIs using a zero-phase FIR filter (53 dB stopband attenuation, maximal ripples in passband 2%, Fig. 1A). We then estimated the functional connectivity between each pair of contacts in slicing windows of length 1 s. Within each time window, the functional connectivity was estimated as the maximum of the absolute value of the cross-correlation for lags between -0.1 and 0.1 s (Fig. 1B). We then defined a strength value (S) for each contact as the mean of its connectivity with all other contacts in each sliding window (Fig. 1C).

The mean strength ($\mathrm{MS}_{i,f,t}$) was then defined for each FOI f, TOI t and contact i as the mean strength in frequency band f across time window t. This step was repeated for each seizure, thus obtaining a mean strength profile across contacts for each seizure, frequency and time of interest (Fig. 1C). To allow for cross-seizure comparison, we normalized mean strength values within each seizure, frequency, and time of interest. We first transformed all MS values using the Fisher z-transform ($\mathrm{MS}'_{i,f,t}$). We then computed the mean $\mu_{f,t}$ and standard deviation $\sigma_{f,t}$ of the transformed values in each frequency f and time window t across contacts. We then defined the normalized mean strength (nMS) for each contact, FOI f and TOI t as the z-score of its Fisher-transformed mean strength (Fig. 1E):

$$\mathrm{nMS}_{i,f,t} = \frac{\mathrm{MS}'_{i,f,t} - \mu_{f,t}}{\sigma_{f,t}} \tag{2}$$

2.6 Statistical analyses

Before performing patient-level analysis, we aimed to assess homogeneity across seizures in each patient. Broadband nMA similarity across seizures was previously shown (Vila-Vidal et al., 2017). Here, we aimed to systematically assess the similarity of nMA and nMS profiles across seizures within each FOI (using the whole seizure as the time window of interest). To do so, we computed the Pearson correlation of nMA between each pair of seizures for each FOI. We then average these values across all pairs of seizures to obtain

a measure of inter-seizure similarity for each patient and FOI. The same procedure was used to quantify the inter-seizure nMS similarity.

Next, we assessed the statistical power of these variables (nMA and nMS) to differentiate between SOZ and non-SOZ contacts at the patient level. To do so, we computed the median nMA (resp. nMS) across seizures and obtained a single value for each contact in each FOI-TOI combination. We then assessed the effect size of differences between between SOZ and non-SOZ contacts using Cohen's d (Cohen, 2016). In addition, we also tested for statistical differences using a non-parametric test (Wilcoxon rank-sum test).

Finally, we compared nMA and nMS as features of a binary classifier for SOZ identification. Specifically, for each variable (nMA and nMS) we computed a receiver operating characteristic (ROC) curve and extracted the area under the curve (AUC) for each FOI-TOI combination. This procedure was done in each patient separately. We then aimed to maximize each classifier's performance under two criteria. The first criterion was to maximize the average performance across patients. This was done by finding the parameter combination (FOI-TOI) which maximized the patient-average AUC for each classifier. The second criterion was to maximize the worst performance across patients. Here, we found the parameter combination (FOI-TOI) which maximized the minimum AUC across patients for each classifier.

2.7 Ethics statement

The study was conducted following the Declaration of Helsinki and informed consent was explicitly obtained from all participants prior to the recordings. All diagnostic and surgical procedures were approved by The Clinical Ethical Committee of Hospital del Mar (Barcelona, Spain).

3 Results

3.1 Computation of nMA and nMS in the time-frequency space

We analyzed 67 seizures from a total of 10 patients to compare the statistical power of a power-based and a connectivity-based biomarker to identify seizure onset contacts across a range of distinct frequencies of interest (FOI) and time windows of interest (TOI). For each seizure and contact, we first computed the time-varying power activation (A) and connectivity strength (S) in each FOI separately. Fig. 2A shows the time evolution of these metrics in the frequency range 3-160 Hz. We then computed each contact's normalized mean activation (nMA) and normalized mean strength (nMS) in each TOI (2B). As an example, Fig. 2B shows the nMA and nMS contact profiles in the frequency range 3-160 Hz and over the whole seizure. In general, SOZ contacts consistently displayed increased power (nMA) and decreased connectivity (nMS) values with respect to other contacts for a wide range of FOI-TOI combinations. Increased nMA indicates the presence of enhanced oscillations at the contact, which in turn becomes less synchronized with the rest of the network, as captured by decreased connectivity.

In addition, for this exemplary patient, both nMA and nMS profiles displayed a high degree of similarity across seizures.

3.2 Assessing seizure similarity within patients

To leverage the data obtained from several recorded seizures for designing a SOZ biomarker, it is relevant to assess the degree of variability of each variable (nMA, nMS) across seizures in each patient. Here, inter-seizure power (resp. connectivity) similarity was evaluated in each patient and FOI by computing the average Pearson correlation of nMA (resp. nMS) multivariate profiles across all pairs of seizures over the whole seizure period (Fig. S1, top). Inter-seizure similarity was shown to be strongly patient-specific. All patients had large nMA and nMS similarities (> 0.6), except for patients P6 and P10. Interestingly, although patient P6 had a medium nMA similarity (0.37 ± 0.06, mean $\pm$ SEM), its nMS similarity remained large (0.76 ± 0.03, mean $\pm$ SEM). Patient P10 had similar nMA and nMS similarities (0.52 ± 0.03, 0.558 ± 0.018, respectively, mean $\pm$ SEM). In addition, nMA and nMS inter-seizure similarity remained high and comparable across frequency bands (≈ 0.8), except in the gamma range of the spectrum, where nMA similarity dropped (0.6 ± 0.1, mean $\pm$ SEM, in high-γ) while nMS similarity remained stable and high (> 0.8). This reinforces the idea that high-frequency nMA may be associated with local neural activity (Vila-Vidal et al., 2023; Buzsáki et al., 2012). Thus, it is more likely to capture the specific electrical patterns of each seizure within patients.

3.3 Exploring parameter-dependent SOZ discrimination

After ensuring a sufficient degree of seizure similarity, we computed the median nMA (resp. nMS) across seizures and tested for statistical differences between SOZ and non-SOZ contacts using each variable. This was initially illustrated using broadband signals and the whole seizure period (Fig. 3). In this example, nMA (nMS) differences were statistically significant in 8 (resp. 7) out of 10 patients. When significant, differences exhibited very large effect sizes ($D > 1$). In patients P2 and P9, neither nMA nor nMS showed statistically significant differences between SOZ and non-SOZ contacts. It is interesting to note that patients P6 and P10, that had less reliable nMA and nMS profiles (Fig. S1, top), also achieved significance in this analysis. Overall, Fig. 3 also shows that patients that are difficult for nMA are also difficult for nMS, suggesting that these two variables might not be able to compensate for each other.

To explore time-frequency combinations yielding significant SOZ discrimination levels, we computed the effect size for each combination of parameters (FOI and TOI) and extracted the mean and standard deviation group values across patients. As shown in Fig. 4, the nMA (power) exhibited on average larger effect sizes with higher variability than nMS (connectivity) for most FOI-TOI combinations. For nMA (Fig. 4, top), the combinations of β band within the range 0-20 s and low-γ band up to 0-5 s maximized the patient-average effect size between SOZ and non-SOZ contacts while keeping moderate variability levels. For nMS (Fig. 4, bottom), the combination of high-γ band within the range 0-30 s maximized the patient-average effect size between SOZ and non-SOZ

contacts but it also yielded the least consistent effect size over the analyzed patients. For completeness, we show in Supplementary Information (Fig. S2) the nMA and nMS effect sizes for each patient.

Overall, in Fig. 4 we generalized the patient-level statistical analysis performed in (Vila-Vidal et al., 2017) to a larger frequency-time space and we applied it to each variable (nMA and nMS) independently. This parallel analysis allowed for a fair statistical comparison between each variable, which might be instrumental to assess the potential of each biomarker to discriminate the SOZ when integrated into classification-based algorithms.

3.4 Classification performance between nMA and nMS

Based on the outcomes of the statistical inference, we asked ourselves how the reported patient-average effect sizes might be translated to proper levels of SOZ discrimination when using practical approaches relying on binary classification algorithms.

To address the above question, we quantified and compared the accuracy of a binary classifier based on the nMA and nMS variables, respectively. In brief, for each variable, patient and combination of parameters (TOI-FOI), we computed the area under the curve (AUC) to measure the classifier's performance. Optimization across parameters' values was achieved under two different criteria. The first criterion relied on maximizing the patient-average performance (Fig. 5A). Hence, the patient-average AUC was computed for each classifier over all TOI-FOI combinations (Fig. 5A, left column). In this case, the maximum (squared in red) was attained in the β band over 0-30 s for the nMA classifier (0.93 ± 0.03, mean $\pm$ SEM across patients, 0.7 minimum across patients) and in low-γ band over 0-30 s for the nMS classifier (0.86 ± 0.04, mean $\pm$ SEM across patients, 0.6, minimum across patients). We also inspected the distribution of AUC across patients arising from each optimal parameter selection (Fig. 5A, right column), for which nMA exhibited a slightly higher performance than nMS.

To guarantee a minimum classification performance satisfied by all patients simultaneously, we defined the second criterion as the maximization of the patient's worst-case performance (Fig. 5B). Hence, we represented the minimum AUC across patients for each classifier over all TOI-FOI combinations (Fig. 5B, left column). In this case, the optimal value (maximizing the patient-minimum AUC) for the nMA classifier shifted to the broadband frequency range over 0-30 s (0.8, minimum across patients). Instead, for the nMS classifier, the optimized value remained at the low-γ band over 0-30 s (0.6, minimum across patients). As expected, the distribution of AUC across patients obtained from optimal selections (Fig. 5B, right column) maintained (nMS) or increased the performance of the patient with minimum AUC (nMA, from 0.7 to 0.8).

For completeness, we show the classification performance of nMA and nMS at the patient level in Fig. S3. The best frequency band for nMA was found to be patient-specific, which might explain why using broadband yields the best results at the group level. In contrast, the best frequency band for nMS remained stable across patients in the low-γ range. This, together with the increased inter-seizure nMS similarity (Fig. S1), indicates that the results might generalize better for nMS than nMA for larger

datasets. The best time window size was also found to be patient-specific, although some consistency was found within each subject across measures (best time windows were similar for nMA and nMS).

In general, the results of the classification accuracy under each criteria showed that the nMA outperformed nMS for most of the TOI-FOI combinations. However, when selecting the optimal combination for each variable, we did not find significant differences in AUC between nMA and NMS in our dataset (n=10, P>0.1) regardless of the employed criterion. More precisely, under optimized conditions, we could differentiate patients in which the classification performance remained approximately the same, patients in which there was a moderate performance variation (AUC difference <0.05) and patients in which there was a notable performance decrease from nMA to nMS (AUC difference >0.05).

In conclusion, the application of the proposed methodology to our available dataset suggests that power-based variables might yield slightly better SOZ identification performance than (single-site) functional connectivity variables such as the connectivity strength. Yet, larger datasets will be needed to characterize such comparison more accurately and to investigate whether the combination of each type of variable can also yield performance improvements. In any event, our methodology is aimed to provide an in-depth and fair comparison analysis between any SOZ discrimination biomarker candidate defined at a single-site level with respect to standard power-based variables to identify novel intracranial EEG features that could strengthen epilepsy presurgical diagnosis.

4 Discussion

In this work we have presented a systematic comparison of different types of biomarkers based on intracranial EEG extracted from peri-ictal periods for SOZ identification in patients with pharmacoresistant epilepsy. Motivated by previous works (Kramer et al., 2008; Geier et al., 2015; Ponten et al., 2007), one of the central goals of the proposed analysis method was to investigate whether standard power-based biomarkers (Vila-Vidal et al., 2017, 2020; Gnatkovsky et al., 2011, 2014; David et al., 2011; Bartolomei et al., 2008) can be outperformed by measures relying on second-order signals' statistics such as measures derived from delayed functional connectivity.

To study the power-connectivity comparison, we here resorted to a rather general measure, the normalized mean activation, (nMA) (Vila-Vidal et al., 2017) as a proxy of power-based biomarkers, and defined an analogous measure, the normalized mean strength (nMS), as a proxy of connectivity-based biomarkers. The nMS corresponds to the mean functional connectivity (cross-correlation) of every contact's signal with the rest of signals over a given time window and frequency band and it can be therefore compared straightforwardly with the nMA. Importantly, the method may be analogously applied to other connectivity or topological measures (Friston, 2011; Bullmore and Sporns, 2009) provided that they are defined at a single-site level (i.e., they can be regarded as vectors of a n-space where n is the number of channels). For each selected measure, the method

validates that normalized measures are consistent across seizures within a single patient and extracts a meaningful median value (over seizures) that is then used to quantify the effect sizes and AUC of the SOZ discrimination over a grid of relevant physiological frequency bands and nested time windows following the seizure onset.

We illustrated the application of our method to analyze the power-connectivity comparison in a dataset of 10 patients with pharmacoresistant temporal lobe epilepsy that accounted for a total of 67 seizures and whose SOZ was clinically validated by epileptologists. The outcomes of our analysis suggest that power-based biomarkers generally perform better than connectivity-based ones. Yet, our results also show that both biomarkers may achieve similar performance levels when appropriately optimized over frequency bands and time windows.

4.1 Seizure homogeneity as initial step for SOZ discrimination

A critical aspect of our method is that it leverages the data from each patient's recurrent seizures for a single SOZ identification, thus accumulating statistical power across seizures to perform inference and classification at a patient level. As demonstrated in a previous work for power activation (Vila-Vidal et al., 2017), we here showed that the values of connectivity strength also attained a very low variance across seizures when they were normalized across contacts (Fig. S1). In particular, there were only a few seizures that substantially deviated from the median value of nMA and nMS, respectively, in a few patients. Overall, the degree of similarity between seizures was very high and this trend was shown to be consistent across patients regardless of the employed measure (Fig. S1).

Assessing seizure homogeneity was key in our method to extract a median value per contact across seizures, which could provide a sufficiently good representation of the patient's ictal activity for each measure. This step was therefore instrumental in performing statistical analysis comparing the activity (power/connectivity) between SOZ and non SOZ contacts per patient (Fig. 3). However, it is due stating that the reported seizure homogeneity of our dataset was possibly favored by the fact that all patients had temporal lobe epilepsy with a clear diagnosed focus. It remained out of the scope of this study to investigate to which degree seizure homogeneity still holds in patients with extra-temporal lobe epilepsy or patients with heterogeneous seizures exhibit foci across different brain areas.

4.2 High activation and low functional connectivity identify SOZ

By inspecting the distribution of nMA and nMS values over patients, we generally reproduced known results in the literature (Fig. 3) pointing to the fact that the SOZ is characterized by significantly higher power activation (Vila-Vidal et al., 2017; Bartolomei et al., 2008) and lower functional connectivity following seizure onset (Kramer et al., 2008). However, this characterization was not uniform among patients when using rather general conditions such as analyzing broadband signals over the whole seizure period. This motivated us to explore how the discrimination of SOZ varied as a func-

tion of clinically relevant frequency and time windows. Indeed, the comparison between nMA and nMS over a grained space of parameters allowed us to investigate in depth its dependence on frequency and time. In particular, we observed that for most of the patients, the SOZ discrimination of nMA was mostly maximized in the low-gamma regime (30-50Hz) over the initial 5 seconds (Fig. 4), which reproduced previous own results (Vila-Vidal et al., 2017). With regard to nMS, we observed that the effect size was likely to increase from low to high frequency and from low to higher time window sizes and it achieved its maximum at the high-gamma band within a time window of 30s following seizure onset. Two factors might explain this frequency and time gradient. First, the frequency increase indicates that functional connectivity is a more representative measure of neural activity when inferred at high-frequency bands since it is known to capture interactions across local neural population from different brain regions (Vila-Vidal et al., 2023; Buzsáki et al., 2012). On the other hand, the temporal increase might reflect that functional connectivity variables operate at a smaller timescale than power-based variables over ictal epochs and they thus require larger time window for estimation.

4.3 Power-based vs. connectivity-based biomarkers for SOZ classification

Upon reviewing the outcomes of our analysis, we may tackle again the question of how connectivity-based biomarkers for SOZ identification compare to power-based biomarkers. Specifically, our results based on the low computational cost measure of cross-correlation reinforce the idea that connectivity measures do not suffice to outperform traditional biomarkers relying on spectral features. Our interpretation behind this behavior is that delayed statistical dependencies, at least at a linear level, do not necessarily reflect information of a connectivity nature such as propagation pathways, but rather they are a measure of signal similarity. This is specially manifested in the SOZ whose connectivity is lower than in the rest of contacts in the gamma band when the ictal spectral patterns become more differentiated from the rest of the signals after seizure onset. Furthermore, detecting seizure propagation across contacts is not a priori an easy task given the limited spatial sampling of intracranial EEG implantation. Hence, further analysis relying on estimations over observed but also non-observed (latent) data are needed to elucidate how to design connectivity-based biomarkers that can capture patterns associated with seizure propagation, thus complementing the information provided by spectral analysis.

4.4 Limitations and other considerations

In this study, we performed a comparison between a power- and a connectivity-based measure to infer the SOZ from iEEG signals. As a result of our analyses, we could establish the optimal parameters for each type of measure in our dataset, but we did not build any joint biomarker that combines both power and connectivity. Further research should investigate how to combine both sources of information, considering that this might vary depending on various factors, such as the epilepsy type, the spectral

features of the seizure onset patterns or the spatial extent of the implantation. In addition, it should be noted that our results are based on the assessment of a very specific connectivity measure derived from cross-correlation. Cross-correlation is defined to capture linear relationships between signals with possible time delays. Other connectivity measures might target other features of the links between signals: nonlinear dependencies, phase-phase couplings or amplitude-amplitude couplings, among others. Some of these measures might capture independent phenomena and, so, our results cannot be generalized. The major limitation of this work, however, is that the power and connectivity analyses were performed retrospectively after the SOZ was defined by clinical electrophysiological criteria and the compromised contacts were determined ad hoc. To ultimately assess the clinical applicability of these and other measures, in future studies, these localization analyses should be performed prospectively in a blinded fashion with respect to the classically defined SOZ

5 Acknowledgements

M.V. and R.Z. were funded by the European Regional Development Funds, Grant/Award Number: CECH/001-P-001682. A. T. C. and M.V. were funded by the Spanish Ministry of Science, Innovation, and Universities (MCIU), Grant/Award Number: PID2020-119072RA-I00/ AEI/10.13039/501100011033. G.D. was supported by the AGAUR research support grant (ref. 2021 SGR 00917) funded by the Department of Research and Universities of the Generalitat of Catalunya, the NODYN Project PID2022-136216NB-I00 financed by the MCIN/AEI/10.13039/501100011033/FEDER, UE., the Ministry of Science and Innovation, the State Research Agency and the European Regional Development Fund and the project NEurological MEchanismS of Injury, and Sleep-like cellular dynamics (NEMESIS) (ref. 101071900) funded by the EU ERC Synergy Horizon Europe.

References

Balatskaya, A., Roehri, N., Lagarde, S., Pizzo, F., Medina, S., Wendling, F., Bénar, C.-G., and Bartolomei, F. (2020). The "connectivity epileptogenicity index" (cei), a method for mapping the different seizure onset patterns in stereoelectroencephalography recorded seizures. *Clinical Neurophysiology*, 131(8):1947–1955.

Bancaud, J. (1980). Surgery of epilepsy based on stereotactic investigations–the plan of the seeg investigation. *Acta neurochirurgica. Supplementum*, 30:25 – 34. Cited by: 40.

Bartolomei, F., Chauvel, P., and Wendling, F. (2008). Epileptogenicity of brain structures in human temporal lobe epilepsy: A quantified study from intracerebral eeg. *Brain*, 131:1818–1830.

Bartolomei, F., Lagarde, S., Wendling, F., McGonigal, A., Jirsa, V., Guye, M., and Bénar, C. (2017). Defining epileptogenic networks: Contribution of seeg and signal

analysis. *Epilepsia*, 58(7):1131 – 1147. Cited by: 307; All Open Access, Green Open Access, Hybrid Gold Open Access.

Bartolomei, F., Wendling, F., Régis, J., Gavaret, M., Guye, M., and Chauvel, P. (2004). Pre-ictal synchronicity in limbic networks of mesial temporal lobe epilepsy. *Epilepsy Research*, 61(1-3):89 – 104. Cited by: 157.

Bullmore, E. and Sporns, O. (2009). Complex brain networks: Graph theoretical analysis of structural and functional systems. *Nature Reviews Neuroscience*, 10:186–198.

Buzsáki, G., Anastassiou, C. A., and Koch, C. (2012). The origin of extracellular fields and currents-eeg, ecog, lfp and spikes. *Nature Reviews Neuroscience*, 13:407–420.

Cardinale, F., Cossu, M., Castana, L., Casaceli, G., Schiariti, M. P., Miserocchi, A., Fuschillo, D., Moscato, A., Caborni, C., Arnulfo, G., and Russo, G. L. (2013). Stereoelectroencephalography: Surgical methodology, safety, and stereotactic application accuracy in 500 procedures. *Neurosurgery*, 72:353–366.

Cohen, J. (2016). A power primer. In Kazdin, A. E., editor, *Methodological issues and strategies in clinical research*, pages 279–284. American Psychological Association.

Courtens, S., Colombet, B., Trébuchon, A., Brovelli, A., Bartolomei, F., and Bénar, C. G. (2016). Graph measures of node strength for characterizing preictal synchrony in partial epilepsy. *Brain Connectivity*, 6(7):530–539. PMID: 27140287.

David, O., Blauwblomme, T., Job, A.-S., Chabards, S., Hoffmann, D., Minotti, L., and Kahane, P. (2011). Imaging the seizure onset zone with stereo-electroencephalography. *Brain*, 134(10):2898 –2911. Cited by: 135; All Open Access, Green Open Access, Hybrid Gold Open Access.

Friston, K. J. (2011). Functional and effective connectivity: A review. *Brain Connectivity*, 1:13–36.

Geier, C., Lehnertz, K., and Bialonski, S. (2015). Time-dependent degree-degree correlations in epileptic brain networks: From assortative to dissortative mixing. *Frontiers in Human Neuroscience*, 9:462.

Gnatkovsky, V., Curtis, M. D., Pastori, C., Cardinale, F., Russo, G. L., Mai, R., Nobili, L., Sartori, I., Tassi, L., and Francione, S. (2014). Biomarkers of epileptogenic zone defined by quantified stereo-eeg analysis. *Epilepsia*, 55:296–305.

Gnatkovsky, V., Francione, S., Cardinale, F., Mai, R., Tassi, L., Russo, G. L., and Curtis, M. D. (2011). Identification of reproducible ictal patterns based on quantified frequency analysis of intracranial eeg signals. *Epilepsia*, 52:477–488.

Gotman, J. and Levtova, V. (1996). Amygdala-hippocampus relationships in temporal lobe seizures: A phase-coherence study. *Epilepsy Research*, 25(1):51 – 57. Cited by: 48.

Guenot, M., Isnard, J., Ryvlin, P., Fischer, C., Ostrowsky, K., Mauguiere, F., and Sindou, M. (2001). Neurophysiological monitoring for epilepsy surgery: The talairach seeg method - indications, results, complications and therapeutic applications in a series of 100 consecutive cases. *Stereotactic and Functional Neurosurgery*, 77:29–32.

Khambhati, A. N., Bassett, D. S., Oommen, B. S., Chen, S. H., Lucas, T. H., Davis, K. A., and Litt, B. (2017). Recurring functional interactions predict network architecture of interictal and ictal states in neocortical epilepsy. *eNeuro*, 4:ENEURO.0091–16.2017.

Kramer, M. A., Kolaczyk, E. D., and Kirsch, H. E. (2008). Emergent network topology at seizure onset in humans. *Epilepsy Research*, 79:173–186.

Lagarde, S., Bonini, F., McGonigal, A., Chauvel, P., Gavaret, M., Scavarda, D., Carron, R., Régis, J., Aubert, S., Villeneuve, N., Giusiano, B., Figarella-Branger, D., Trebuchon, A., and Bartolomei, F. (2016). Seizure-onset patterns in focal cortical dysplasia and neurodevelopmental tumors: Relationship with surgical prognosis and neuropathologic subtypes. *Epilepsia*, 57:1426–1435.

Mierlo, P. V., Carrette, E., Hallez, H., Raedt, R., Meurs, A., Vandenberghe, S., Roost, D. V., Boon, P., Staelens, S., and Vonck, K. (2013). Ictal-onset localization through connectivity analysis of intracranial eeg signals in patients with refractory epilepsy. *Epilepsia*, 54:1409–1418.

Mierlo, P. V., Papadopoulou, M., Carrette, E., Boon, P., Vandenberghe, S., Vonck, K., and Marinazzo, D. (2014). Functional brain connectivity from eeg in epilepsy: Seizure prediction and epileptogenic focus localization. *Progress in Neurobiology*, 121:19–35.

Munari, C. and Bancaud, J. (1985). The role of stereo-electroencephalography (seeg) in the evaluation of partial epileptic seizures. pages 267–306. Butterworths.

Murphy, P. M., von Paternos, A. J., and Santaniello, S. (2017). A novel hfo-based method for unsupervised localization of the seizure onset zone in drug-resistant epilepsy. pages 1054–1057. IEEE.

Nahvi, M., Ardeshir, G., Ezoji, M., Tafakhori, A., Shafiee, S., and Babajani-Feremi, A. (2023). An application of dynamical directed connectivity of ictal intracranial eeg recordings in seizure onset zone localization. *Journal of Neuroscience Methods*, 386:109775.

Perucca, P., Dubeau, F., and Gotman, J. (2014). Intracranial electroencephalographic seizure-onset patterns: Effect of underlying pathology. *Brain*, 137:183–196.

Ponten, S. C., Bartolomei, F., and Stam, C. J. (2007). Small-world networks and epilepsy: Graph theoretical analysis of intracerebrally recorded mesial temporal lobe seizures. *Clinical Neurophysiology*, 118:918–927.

Talairach, J., Bancaud, J., Szikla, G., Bonis, A., Geier, S., and Vedrenne, C. (1974). Approche nouvelle de la neurochirurgie de l'epilepsie. méthodologie stéréotaxique et résultats thérapeutiques. 1. introduction et historique [new approach to the neurosurgery of epilepsy. stereotaxic methodology and therapeutic results. 1. introduction an. *Neuro-Chirurgie*, 20:1–240.

Varotto, G., Tassi, L., Franceschetti, S., Spreafico, R., and Panzica, F. (2012). Epileptogenic networks of type ii focal cortical dysplasia: A stereo-eeg study. *NeuroImage*, 61:591–598.

Vila-Vidal, M., Enríquez, C. P., Principe, A., Rocamora, R., Deco, G., and Campo, A. T. (2020). Low entropy map of brain oscillatory activity identifies spatially localized events: A new method for automated epilepsy focus prediction. *NeuroImage*, 208:116410.

Vila-Vidal, M., Khawaja, M., Carreño, M., Roldán, P., Rumià, J., Donaire, A., Deco, G., and Tauste Campo, A. (2023). Assessing the coupling between local neural activity and global connectivity fluctuations: Application to human intracranial electroencephalography during a cognitive task. *Human Brain Mapping*, 44(3):1173–1192.

Vila-Vidal, M., Principe, A., Ley, M., Deco, G., Tauste Campo, A., and Rocamora, R. (2017). Detection of recurrent activation patterns across focal seizures: Application to seizure onset zone identification. *Clinical Neurophysiology*, 128.

Vila-Vidal, M. and Tauste Campo, A. (2023). *Mapping Epileptic Networks with Scalp and Invasive EEG: Applications to Epileptogenic Zone Localization and Seizure Prediction*, page 99–126. Cambridge University Press.

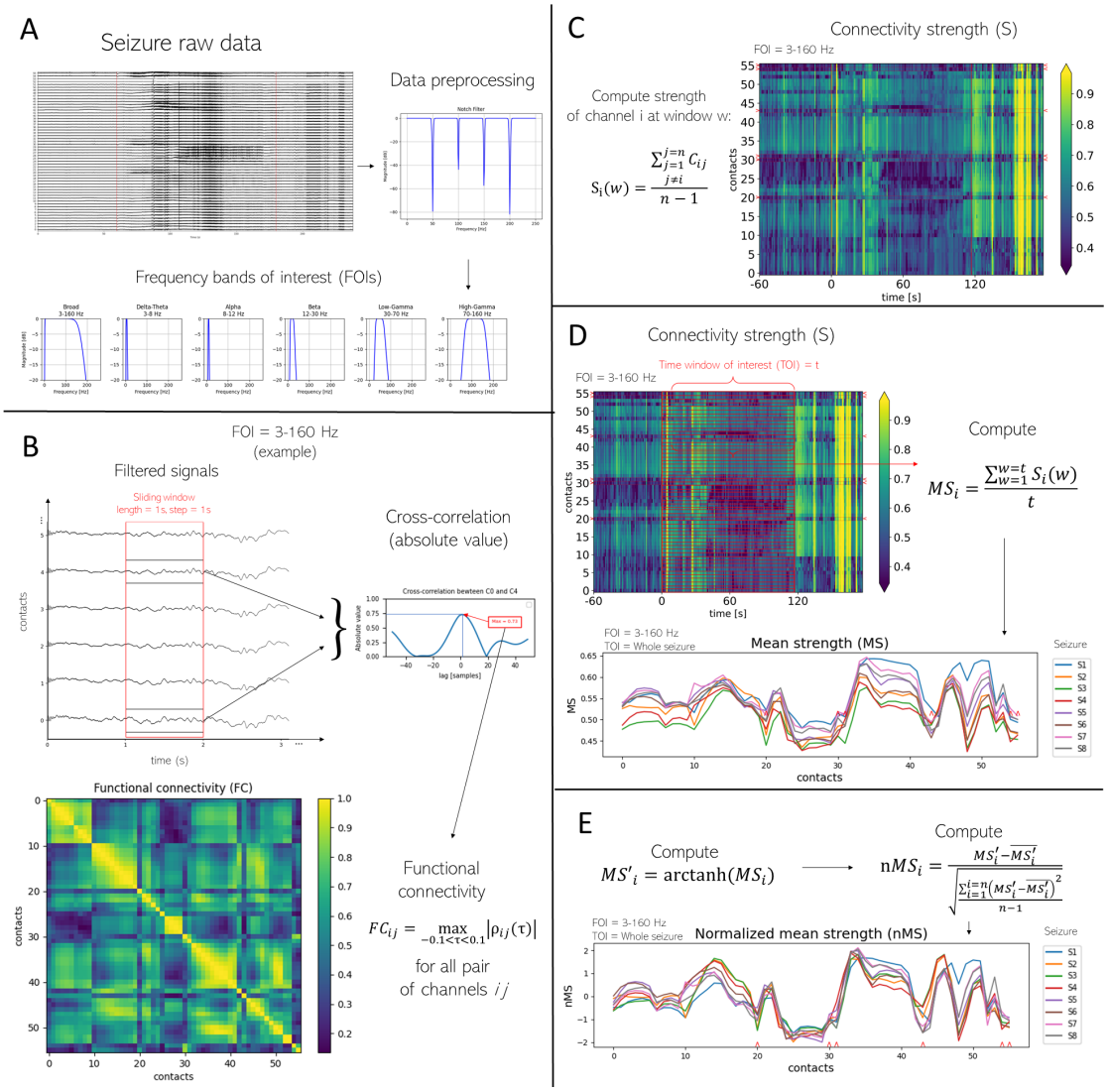

Figure 1. Functional connectivity-based biomarker: normalized mean strength (nMA) A. Data preprocessing and canonical band filtering. Raw signals were notch-filtered to remove the power line interference at 50 and its multiples. Vertical red lines mark seizure onset and offset. Seizure onset is used as the reference time (0 s). Signals were then band-pass filtered in six frequencies of interest (FOI), including 5 canonical bands and a broadband component: broadband: 3-160 Hz; δ-θ: 3-8 Hz; α: 8-12 Hz; β: 12-30 Hz; low-γ: 30-70 Hz; high-γ: 70-160 Hz. Artifacted noisy channels were visually identified in this step and removed for the following steps. **B.** Time-varying functional connectivity. Using a sliding window approach (window length and step of 1 s), we computed the time-varying functional connectivity (FC) for each pair of contacts. The functional connectivity was estimated as the maximum absolute value of the cross-correlation across lags ranging from -0.1 to 0.1 s. **C.** Time-varying connectivity strength. The connectivity strength (S) was computed as the mean of the functional connectivity between each channel and the rest of the channels for each time window. **D.** Mean strength in each time window of interest. For each contact and time window of interest (TOI), we computed the mean connectivity strength (MS) as the mean connectivity strength in the TOI. In particular, we explored the following TOIs: 0-1s, 0-2s, 0-3s, 0-4s, 0-5s, 0-10s, 0-20s, 0-30s, and whole seizure period. This procedure was repeated for each seizure. **E.** Normalized mean strength. To allow comparisons across seizures per patient, MS values were Fisher transformed and normalized (z-score) in each seizure separately, thus obtaining a normalized mean strength (nMS) for each contact over a given seizure. For each patient's data, steps B-E were repeated for all FOIs and TOIs.

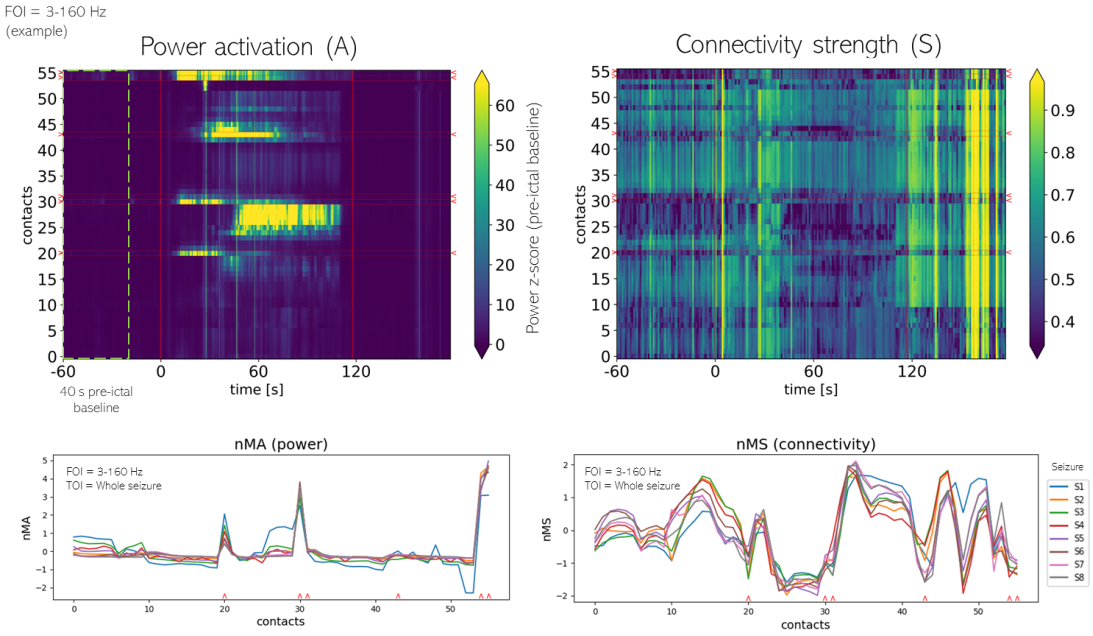

Figure 2. Power- and connectivity-based biomarkers evaluated in 3-160 Hz (FOI) and over the whole seizure period (TOI) in an exemplary seizure of patient P1. Top panels display the broadband (3-160 Hz) time-varying power activation (A, top-left) and connectivity strength (S, top-right). Power values are expressed as a z-score with respect to a baseline distribution built by pooling all contacts' power values in the time period from -60 s to -20 s. Connectivity strength (S) measures the average functional connectivity of each contact with respect to all other contacts and is computed using a sliding window approach (window length and step of 1 s). Seizure onset and offset times are marked with red vertical lines. The clinically annotated seizure onset zone (SOZ) contacts are marked in red next to the y-axis. Bottom panels display the normalized mean activation (nMA, bottom-left) and normalized mean strength (nMS, bottom-right) computed over the whole seizure period for all seizures of patient P1. Clinically annotated SOZ contacts are marked in red on the x-axis. As previously shown with nMA, the nMS profile displays a high degree of similarity across seizure. SOZ contacts consistently display increased power (nMA) and decreased connectivity (nMS) with respect to other contacts.

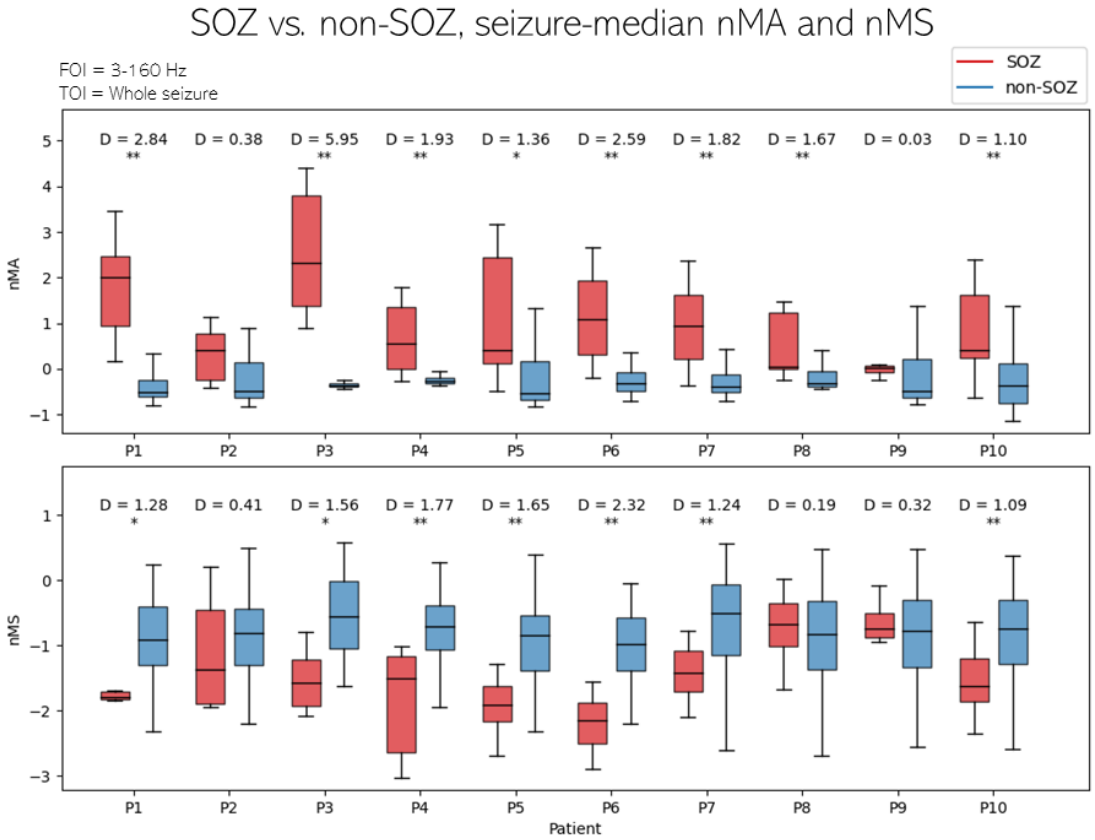

Figure 3. SOZ discrimination with nMA and nMS for an example of parameters of interest (FOI = broadband, 3-160 Hz, TOI = whole seizure period). Boxplots showing the distribution of seizure-median nMA (top) and nMS (bottom) values across SOZ and non-SOZ contacts for each patient. nMA and nMS were estimated for each contact and seizure of patient P1 in 3-160 Hz (FOI) and over the whole seizure period (TOI). Seizure-median nMA and nMS values were obtained for each contact. Differences between SOZ and non-SOZ contacts were tested for statistical significance using a Wilcoxon rank-sum test (** $P < 0.001$, * $P < 0.01$). Effect sizes were evaluated using Cohen's d (reported above each comparison). For this combination of frequency band and time window of interest, all nMA differences were statistically significant ($P < 0.01$) in all cases except in patients P2 and P9. nMS differences were statistically significant ($P < 0.01$) in all cases except in patients P2, P8, P9. When significant, differences exhibited very large effect sizes ($D > 1$). Group (SOZ/non-SOZ) sample sizes for each patient were 6/48, 9/58, 6/50, 11/67, 8/77, 9/90, 11/96, 9/86, 4/120, 13/109.

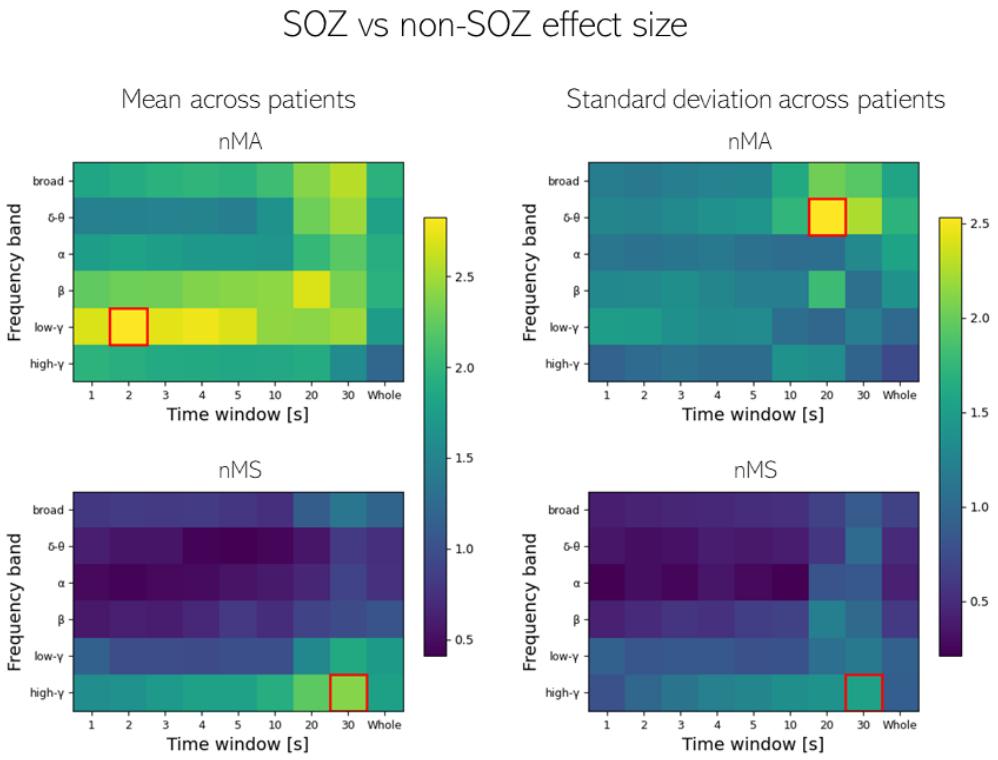

Figure 4. SOZ discrimination (effect size) across patients with nMA and nMS as a function of different FOIs and TOIs. nMA and nMS were estimated for each contact and seizure, and for each combination of FOI (broadband: 3-160 Hz, δ-θ: 3-8 Hz, α: 8-12 Hz, β: 12-30 Hz, low-γ: 30-70 Hz, and high-γ: 70-160 Hz) and TOI (0-1s, 0-2s, 0-3s, 0-4s, 0-5s, 0-10s, 0-20s, 0-30s, and whole seizure period). Seizure-median nMA and nMS values were then obtained obtained for each contact, FOI and TOI. The size of differences between SOZ and non-SOZ contacts with nMA and nMS was quantified using Cohen's d in each FOI and TOI independently. This procedure was repeated for each patient, thus obtaining a distribution of 10 effect size values (one per patient) for each FOI and TOI. Color maps show the mean (left) and standard deviation (right) of nMA (top) and nMS (bottom) effect sizes across patients for every FOI (y-axis) and TOI (x-axis). nMA (power) exhibited on average larger effect sizes with hifger variability than nMS (connectivity) for most FOI-TOI combinations. For nMA (top), the combinations of β band within the range 0-20 s and low-γ band up to 0-5 s maximized the effect size between SOZ and non-SOZ contacts. For nMS, the combination of high-γ band within the range [0,30] s maximized the effect size between SOZ and non-SOZ contacts. See Supplementary Information (A) for patient-specific nMA and nMS effect sizes.

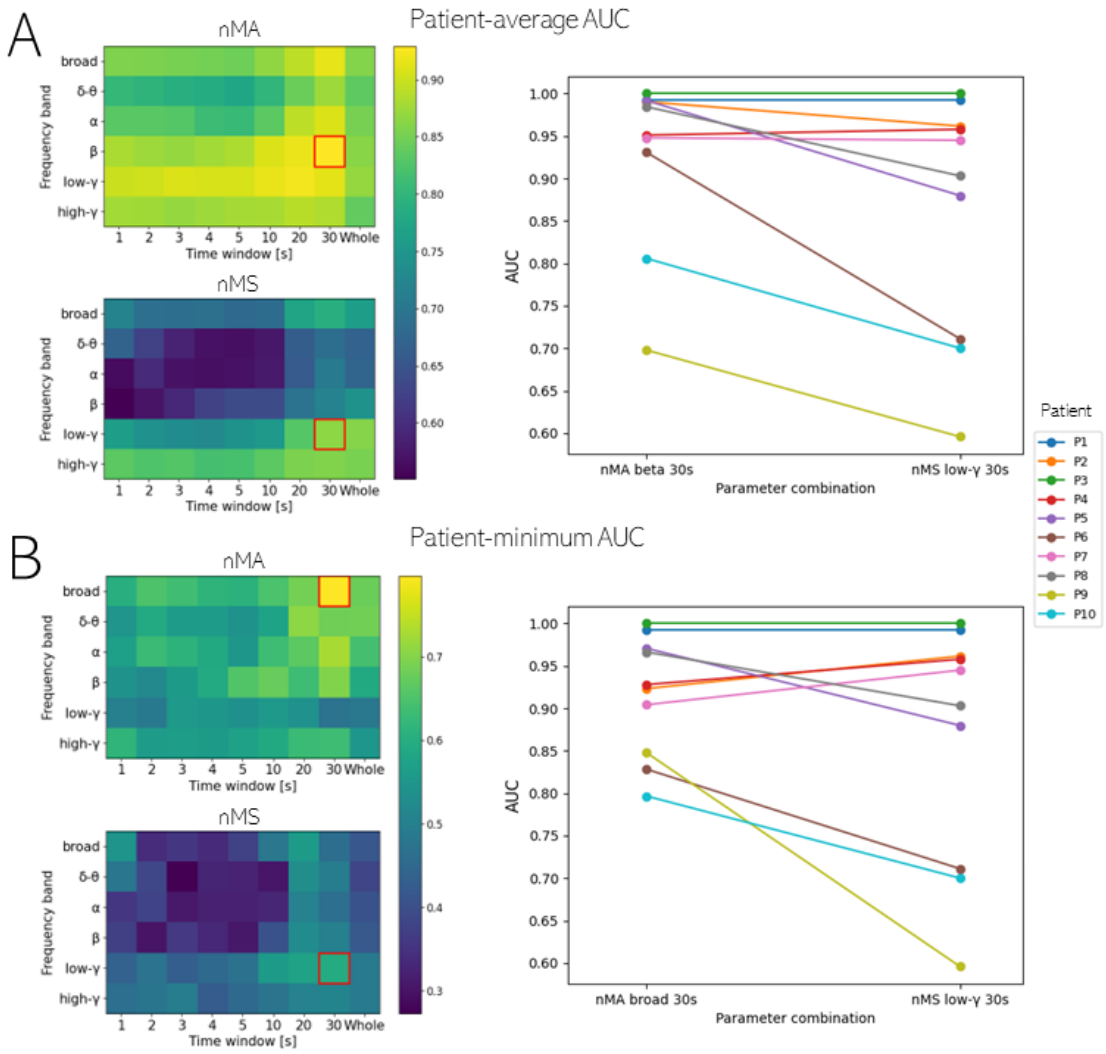

Figure 5. SOZ vs non-SOZ classification performance based on nMA and nMS values. A. Parameter optimization (over a pre-defined time-frequency grid) based on patient-average performance. The left panel shows patient-average AUC values for the SOZ classifier based on seizure-median nMA (top) and seizure-median nMS (bottom). The maximum value of patient-average AUC was found in the β band over 0-30 s for nMA, while in low-γ band over 0-30 s for nMS. The right panel shows the AUC values obtained in each patient with the nMA and nMS classifiers when using the optimal parameter combinations, respectively. **B.** Parameter optimization (over a pre-defined time-frequency grid) based on patient-minimum performance. The optimization criterion used here is based on maximizing the worst-case scenario. The left panel shows patient-minimum AUC values for the SOZ classifier based on seizure-median nMA (top) and seizure-median nMS (bottom). The maximum value of patient-worst performance was found when using broadband signals over 0-30 s for nMA. In contrast, maximization of patient-worst performance with nMS was achieved at the low-γ band and 0-30 s, the same combination found in (A). The right panel shows the AUC values obtained in each patient with the nMA and nMS classifiers when using the optimal parameter combinations. In addition, the time window 0-30 s was the AUC-maximizing time window in all cases. AUC values for the obtained combinations were all above 0.6 for nMS and above 0.7 for nMA. Differences between AUC values were not statistically significant between nMA and nMS (Wilcoxon rank-sum test).

A Supplementary Information

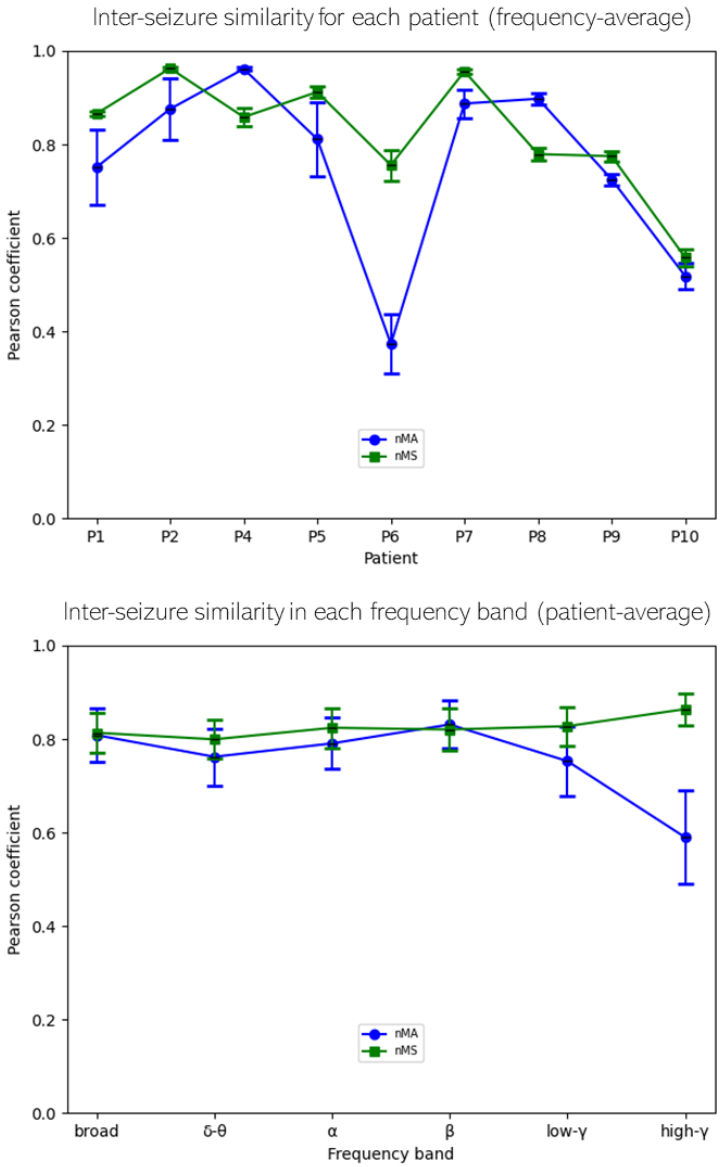

Figure S1. Inter-seizure similarity across patients (frequency-average) and across frequency bands (patient-average). The mean Pearson coefficient was computed to assess the similarity of nMA (resp. nMS) contact profiles across seizures. Similarities across patients with error bars related to variability across frequency bands (top) and similarities across frequency bands with error bars related to variability across patients (bottom) are shown for a time window of the whole seizure period. Patient 3 was excluded in this figure because it only had one seizure, and therefore no inter-seizure variability could be computed. For inter-seizure variability across patients (top), all patients had mean similarities above 0.5 except for nMA in patient 6. Distribution of similarities across frequency bands (bottom) was similar between nMA and nMS except for low- and high-γ frequency bands.

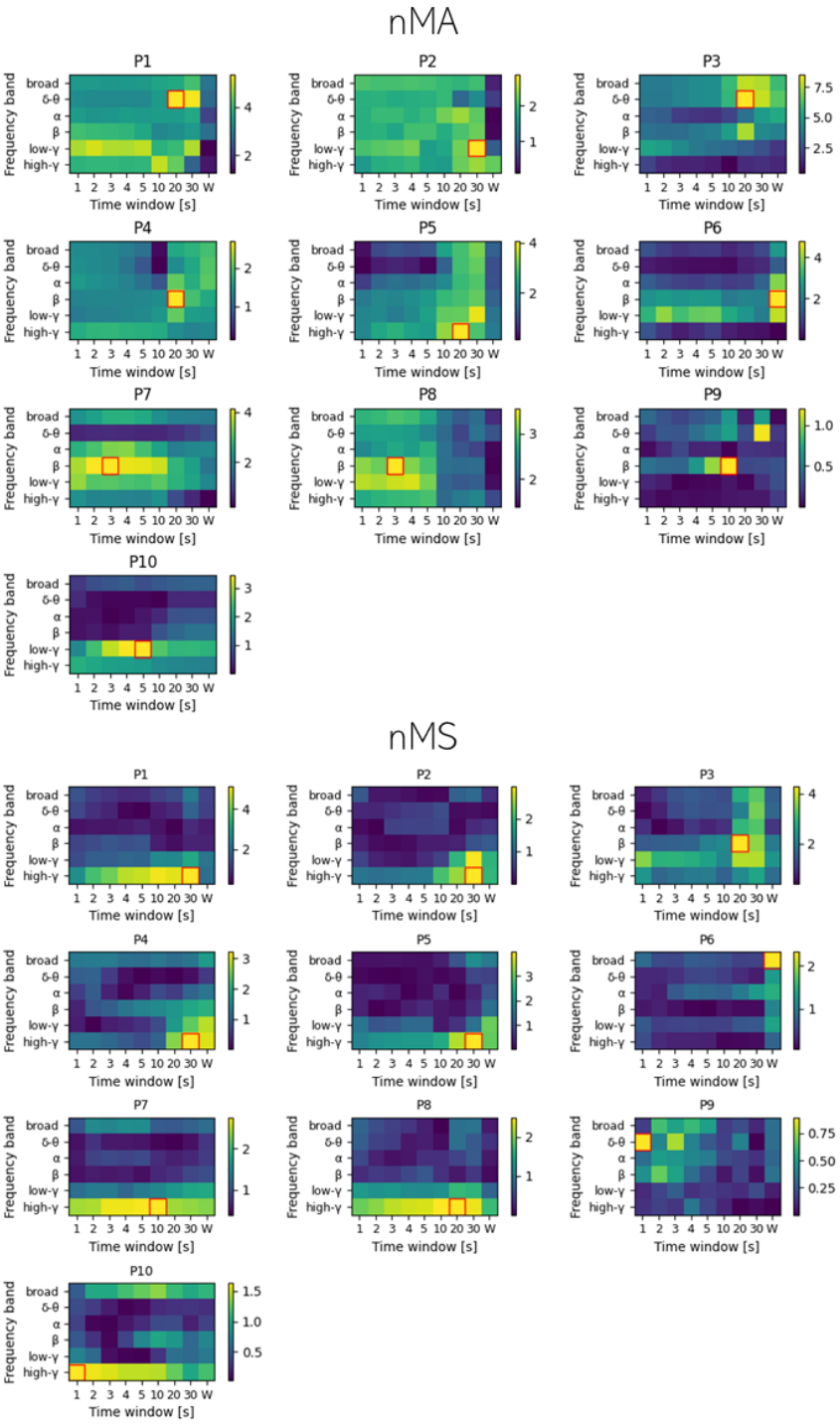

Figure S2. SOZ discrimination (effect size) for each patient with nMA and nMS as a function of different FOIs and TOIs Color maps show the seizure-median nMS (top) and nMA (bottom) effect size (Cohen's d) values across SOZ and non-SOZ groups for the different frequency bands (y-axis FOIs: broadband: 3-160 Hz, δ-θ: 3-8 Hz, α: 8-12 Hz, β: 12-30 Hz, low-γ: 30-70 Hz, and high-γ: 70-160 Hz) and time windows (x-axis TOIs: 0-1s, 0-2s, 0-3s, 0-4s, 0-5s, 0-10s, 0-20s, 0-30s, and whole seizure period). For nMS (connectivity), high-γ frequency band and long time windows ($>$ 20 s) maximized effect size in 7 out of 10 patients. Effect size values were greater in nMA (color bar scales) than in nMS for all patients except for patient 4. In nMA, mid-high frequency bands (beta and low-gamma) maximized effect size in 7 out of 10 patients, while effect size-maximizing time windows were different across patients.

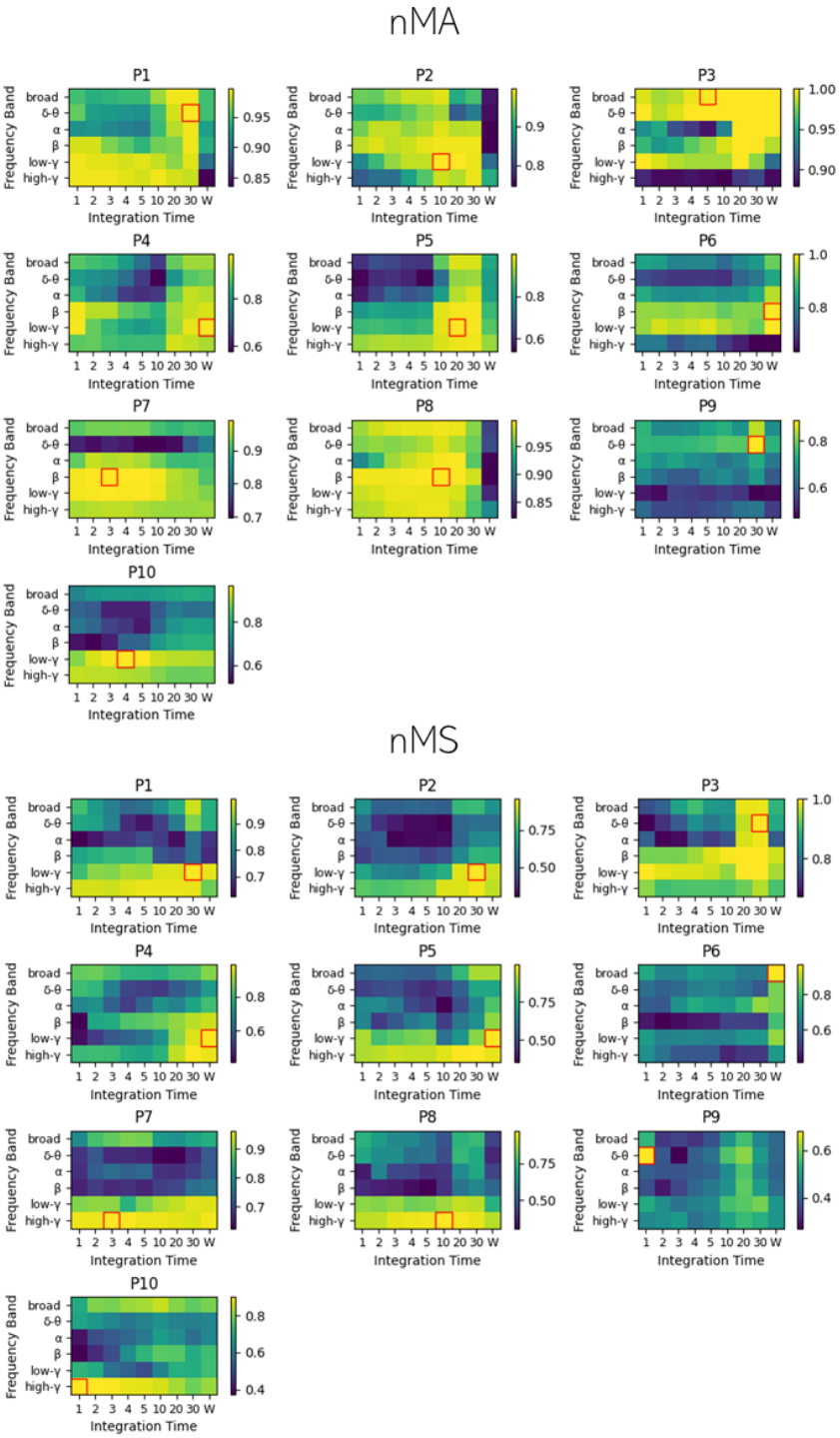

Figure S3. SOZ discrimination (AUC) for each patient with nMA and nMS as a function of different FOIs and TOIs Color maps show the seizure-median nMS (top) and nMA (bottom) AUC values across SOZ and non-SOZ groups for the different frequency bands (y-axis FOIs: broadband: 3-160 Hz, δ-θ: 3-8 Hz, α: 8-12 Hz, β: 12-30 Hz, low-γ: 30-70 Hz, and high-γ: 70-160 Hz) and time windows (x-axis TOIs: 0-1s, 0-2s, 0-3s, 0-4s, 0-5s, 0-10s, 0-20s, 0-30s, and whole seizure period). For nMS (connectivity), high frequency bands (high- and low-γ) and long time windows ($>$ 20 s) maximized effect size in 6 out of 10 patients. AUC values were greater in nMA (color bar scales) than in nMS for all patients. In nMA, mid-high frequency bands (beta and low-gamma) maximized AUC in 7 out of 10 patients, while AUC-maximizing time windows were different across patients.

Table 1. Main data of patients included in the study.

Patient	Gender /Age	Epilepsy	Side	Duration (years)	Electrodes (left)	Number of recording sites	Number of sites within the SOZ	Analyzed Seizures	MRI	Surgery	Treated structure	Outcome (Engel's class)	Follow-up (years)
1	F/27	TLE	R	10	5(0)	54	6	8	negative	R TATL	temporal pole, amygdala and head of hippocampus	Ia	6
2	F/30	TLE	L	25	7(7)	67	9	8	negative	SAH	temporal pole, inferior half of amygdala and anterior 1/3 of hippocampus	Ic	6
3	F/55	TLE	L	40	6(6)	56	6	1	negative	L TATL	temporal pole, amygdala and head of hippocampus	Ib	6
4	M/26	TLE	R	11	7(0)	78	11	7	R amygdala enlargement	RF-TC	temporal pole, amygdala, entorhinal cortex and fusiform gyrus	Rp (Ib)	4
5	M/40	TLE	L	2	8(8)	85	8	7	L temporal polar blurring	RF-TC	temporal pole and hippocampal head	uRp (III)	4
6	F/52	TLE	L	45	10(8)	99	9	6	gliosis near R crainotomy	L TATL	temporal pole, inferior half of amygdala and anterior 1/3 of hippocampus	Ib	5
7	F/40	TLE	L	16	10(8)	107	11	10	L posterior hippocampal lesion	L TATL	2/3 of amygdala and anterior 2/3 of hippocampus	III	6
8	M/29	TLE	R	9	0(0)	95	9	8	negative	NO		Ia	5
*9	M/43	TLE	R	42	15(0)	124	4	5	FCDIIIa. Arachnoid Cyst.	R TATL	temporal pole, amygdala and 2/3 of hippocampus	Ia	3
10	M/20	TLE	L	12	15(15)	122	13	7	negative	RF-TC	anterior and posterior superior temporal gyrus, transverse temporal gyrus and supramarginal gyrus	Rp (Ib)	4

F = female; M = male; TLE = temporal lobe epilepsy; R = right; L = left; FC = frontal cingulate; R FC = right frontal cingulate; L FC = left frontal cingulate; A = amygdala; Ha = anterior hippocampus; Hp = posterior hippocampus; TP = temporal pole; EC = entorhinal cortex, OFCm = mesial orbitofrontal cortex; TGi = inferior temporal gyrus; PHCp = posterior parahippocampal cortex; W = Wernicke's area; TOJ = temporal occipital junction; FBC = frontal basal cortex; MS = motor strip; TCl = lateral temporal cortex; OCm = mesial occipital cortex; FS = focal seizure; w = with; wo = without; CA = consciousness alteration; TATL: Tailored anterior temporal lobectomy; RF-TC = Radiofrequency thermocoagulation; SAH = Selective amygdalohyppocampectomy; Rp = Responsive; uRp = Unresponsive; NO = not-operated. *Patient 9 was initially responsive to RF-TC but experienced seizure relapse two years after the procedure. He then underwent resective surgery, after which he achieved seizure freedom (Engel I) with a follow-up of 3 years.